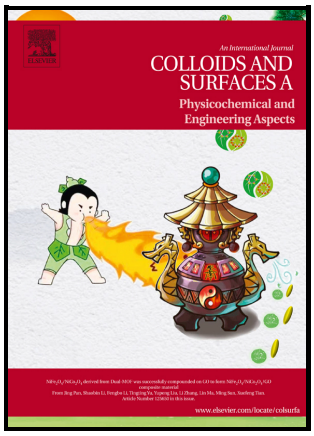

Enhanced electromagnetic wave absorption of magnetite-spinach derived carbon composite

Yuan Yi, Chunzhi Zhao, Hamukwaya L. Shindume, Juanna Ren, Leilei Chen, Hua Hou, Mohamed M. Ibrahim, Zeinhom M. El-Bahy, Zhanhu Guo, Zengying Zhao, Junwei Gu

PII: S0927-7757(24)01010-0

DOI: https://doi.org/10.1016/j.colsurfa.2024.134149

Reference: COLSUA134149

To appear in: *Colloids and Surfaces A: Physicochemical and Engineering Aspects*

Received date: 23 February 2024
Revised date: 25 April 2024
Accepted date: 30 April 2024

Please cite this article as: Yuan Yi, Chunzhi Zhao, Hamukwaya L. Shindume, Juanna Ren, Leilei Chen, Hua Hou, Mohamed M. Ibrahim, Zeinhom M. El-Bahy, Zhanhu Guo, Zengying Zhao and Junwei Gu, Enhanced electromagnetic wave absorption of magnetite-spinach derived carbon composite, *Colloids and Surfaces A: Physicochemical and Engineering Aspects,* (2024) doi:https://doi.org/10.1016/j.colsurfa.2024.134149

Enhanced electromagnetic wave absorption of magnetite-spinach derived carbon composite

Yuan Yi [a, #], Chunzhi Zhao [a, #], Hamukwaya L. Shindume [a, b], Juanna Ren[c,d], Leilei Chen [a], Hua Hou[c], Mohamed M. Ibrahim[e], Zeinhom M. El-Bahy[f], Zhanhu Guo [d,*], Zengying Zhao [a,*], and Junwei Gu[h,*]

[a.] *School of Science, China University of Geosciences Beijing, Beijing 100083, PR China*

[b.] *School of Engineering and the Built Environment, University of Namibia, Ongwediva 33004, Namibia*

[c] *College of Materials Science and Engineering, Taiyuan University of Science and Technology, Taiyuan, 030024, China*

[d.] *Mechanical and Construction Engineering, Faculty of Engineering and Environment, Northumbria University, Newcastle Upon Tyne, NE1 8ST, UK*

[e] *Department of Chemistry, College of Science, Taif University, P.O. Box 11099, Taif 21944, Saudi Arabia*

[f] *Department of Chemistry, Faculty of Science, Al-Azhar University, Nasr City 11884, Cairo,* Egypt

[h] *Shaanxi Key Laboratory of Macromolecular Science and Technology, School of Chemistry and Chemical Engineering, Northwestern Polytechnical University, Xi'an, Shaanxi 710072, China*

*Corresponding author, E-mail address: zhaozy@cugb.edu.cn, (Z. Zhao); zhanhu.guo@northumbria.ac.uk (Z. Guo); gjw@nwpu.edu.cn (J. Gu)

#They are the co-first authors.

Abstract

The high density, high cost, and environmental pollution hinder the application of iron-based electromagnetic wave-absorbing materials. Although bio-carbon is a green and lightweight dielectric wave-absorbing material, the wave-absorbing performance of bio-carbon is still limited. This work successfully combined magnetite Fe_3O_4 with porous carbon derived from spinach stem using hydrothermal and calcination methods. This process optimizes the matching of the dielectric constant and magnetoconductivity of the as prepared composite material, resulting in a significant improvement in electromagnetic microwave absorption capacity. XRD, SEM, TEM, XPS, VSM and EMW absorption network analyzer are used to detect and characterize the samples. The composite material shows a excellent minimum reflection loss value of -48.81 dB and an efficacious absorption bandwidth of 4.73 GHz at the optimal raw material ratio. The tests also show the porous structure of the sample with the coercivity and saturation magnetization of 29.36 Oe and 10.75 emu/g, respectively. The test results indicate that the excellent electromagnetic wave absorption is due to the synergistic effect of multiple reflection, Debye relaxation, and interfacial polarization. This Fe_3O_4-bio-carbon composite is cheap and simple to prepare, and it also has excellent wave absorption performance. Therefore, it shows great application potential in civilian and military electromagnetic wave absorption fields.

Keywords: Bio-carbon; Fe_3O_4; Spinach; Wave-absorbing material.

1. Introduction

Due to the flourishing advance of electronics and wireless communication [1-5], electromagnetic waves (EMW) are used in increasing civilian and military equipment [6-8]. This has also raised many serious issues, for example, interference with electronic devices and hazards to human health [9-12]. In addition, military stealth materials also have problems with electromagnetic pollution, such as the films used on fighter aircraft and unmanned aerial vehicles [13, 14]. It is an exigent issue to reduce electromagnetic wave pollution using good performance materials. In order to address this problem, it is crucial to prepare electromagnetic wave absorbing material with lightweight materials, strong absorption ability, and effective absorption bandwidth [15].

The characteristics of electricity and magnetism of a material are the main factors in determining its electromagnetic absorbing property [16-18]. The magnetic loss wave-absorbing materials generally include ferrites [19], magnetic metal oxides [20-22], magnetic metals (for example, Fe, Co and Ni) and alloys (FeCo) [23-26], while dielectric loss wave-absorbing materials are mainly conductive polymers [27-29], metal [30-32], sulfide [33, 34], and carbon-based materials [35-41]. Even though these monocomponent materials show certain EMW absorbing qualities, they cannot satisfy the practical need for the ideal absorbing material [42-44]. This is because its absorption loss mechanism is relatively single and electromagnetic parameters cannot be accurately controlled [45-47].

Bio-carbon materials have the advantages of being lightweight, having high dielectric loss, large specific surface area, and stable chemical properties, which make them an ideal option for microwave absorption [48, 49]. For example, the research on carbon nanotubes and graphene has become a research hotspot in recent years [50-53]. However, the carbon nanotubes and graphene are not cheap and simple in the preparation process [54-57]. Besides, the preparation processes of carbon nanotubes and graphene, such as chemical vapor deposition, hummer method, and arc discharge, etc., always need high energy [58]. Biomass can be a renewable, environmentally-

friendly resource that is abundantly available [59-62]. Bio-carbon can be fabricated from biomass by a simple heat treatment process [63-69]. Therefore, it has been considered a new and economically feasible electromagnetic wave-absorbing material. However, bio-carbon itself can only provide limited dielectric losses in the wave-absorbing process.

Compounding functional materials with bio-carbon is advantageous to improve microwave absorption. For instance, cobalt preparation for carbon fibers uses cotton materials by Li et al. [70]. Composing Co with carbon material creates a good impedance matching. When 33% is filled, a large range of minimum reflection loss (RL) can be lower than -10 dB. Its effective absorption range is between 11.3-18 GHz, and this range is close to the complete Ku range (12 to 18 GHz). Zhao et al. also prepared a Co@crystalline carbon@carbon aerogel ternary composite based on biomass of alginate, and the absorption performance can reach -43 dB at a 10% filling rate [71].

Especially in recent years, the composite of bio-carbon with iron-based materials has attracted much attention due to their simplicity in preparation, low cost, harmlessness to the environment, good impedance matching, and synergistic effect of multi-loss mechanisms [72, 73]. For instance, Gao et al. prepared a composite of iron oxide and nutshell carbon by solvothermal method [74]. Compared with pure Fe_3O_4 and single nutshell carbon, the Fe_3O_4/bio-carbon composite showed better microwave absorption. Electrical properties provided by the biocarbon are the reason for the increased wave absorption rate. Besides, the high density and easy agglomeration of Fe_3O_4 can also be addressed by coupling with carbon materials. The large saturation magnetization of Fe_3O_4 can provide high composite permeability values for carbon materials. This can be coordinated with the electrical conductivity of the bio-carbon [75-77]. For example, Liang et al. prepared a Fe_3O_4-FeO-biochar material. This hydrothermal and calcination reaction is simple and easy to implement. The as-prepared material has an absorption bandwidth of 6.1 GHz at 1.9 mm and an RL of -40.8 dB [78]. Meng et al. prepared Fe_3O_4 composite nanoparticles (NP) shielded with an ultra-thin carbon layer (Fe_3O_4/C) using a simple high-temperature liquid phase method and then a high-temperature steam carbonization method. By controlling the Fe_3O_4 size, the interface contact area for Fe_3O_4 and carbon layer changes significantly, thereby quantifying and controlling the interface

polarization behavior.

Although these materials have shown enhanced EMW absorption performance to some extent, most of them still do not meet the high strength and wideband requirements in practical application. There still exist problems such as self-activation difficulty, high cost and easy to cause pollution. Spinach stem has an inherent micro-scale porous tissue structure compared to other biomass [79]. It can also be activated by the embedded alkali metal elements without an external activator in its biocarbon preparation process. The spinach stem carbonization process can form a hierarchical porous structure. This makes its wave absorbing composite superior to those of most other biomass chars, such as bagasse [80], and shaddock peel [81], etc. As far as we know, there still have no reports about the preparation and wave absorbing of the composite of Fe_3O_4 and spinach stem-derived biocarbon. It can be expected that this composite may have better EMW absorption performance. The addition of Fe_3O_4 can make the composite has natural resonance and exchange resonance effect, then enhance electromagnetic wave dissipation and achieve a good impedance matching. Therefore, its electromagnetic wave absorption property is excellent compared with the above mentioned materals. A one-step carbonization method was used to prepare bio-carbon with spinach stems as a raw materials, and then it was compounded with ferric chloride hexahydrate by hydrothermal method. The typical sample shows the strong microwave absorption intensity of -48 dB and the efficacious absorption bandwidth was 4.73 GHz. Besides, the mechanism were also explored by a series tests and characteristics. The the main objective of this work is to prepare the novel Fe_3O_4 - spinach stem biocarbon composite and to provide a new sight to achieve sustainable and effective approach for the use of bio-carbon in EMW absorption application.

2. Experimental section

2.1. Preparation of samples

The bio-carbon were derived from spinach stem. A typical preparation procedure is as follows: spinach stems were washed, dried, and then heated at 600 ℃ at 5 ℃ / min for 2 h under a gas flow of N_2 (190 s.c.c.m.). After natural cooling to room temperature, the calcined sample was cleaned

with distilled water and dried under vacuum under 60 ℃, with the resulting specimen labeled as 0 FOC. The above 150 mg bio-carbon was added to 20 ml of ethylene glycol and stirred at room temperature for 30 min. Then 0.0541 g ferric hexahydrate, 1.2 g sodium acetate and 0.2 g sodium citrate were sealed in a 100 ml stainless-steel autoclave maintained at 200 °C for 10 h. The product were cooled to room temperature naturally, and followed by washing with pure water and absolute ethanol several times and then drying at 80 °C for 10 h. The as prepared Fe_3O_4/C composite can be changed by adjusting the amount of ferric chloride and sodium acetate. The different samples were labeled as xFOC with the x be 0.2, 0.4, 0.6. For example, the sample can be named 0.2FOC when there are 0.054 g (0.20 mmol) ferric chloride and 1.2 g sodium acetate in the raw material.

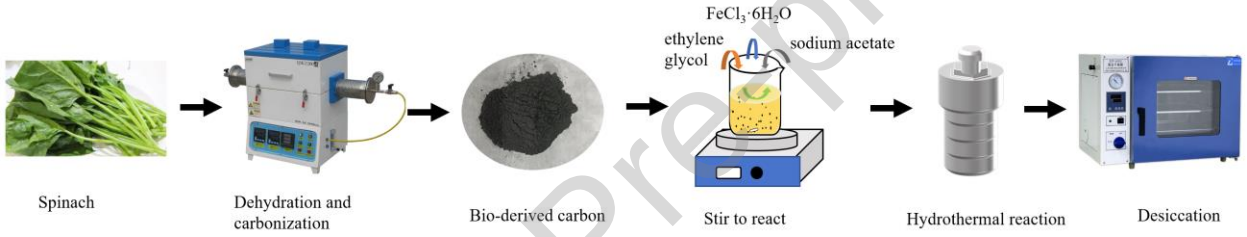

Scheme 1. The preparation of the samples.

2.2. Characterization

Scanning electron microscopy (SEM, Hitachi S-4800) was used to analyze the sample microstructure. A transmission electron microscope (TEM, Hitachi H-8100) was used to determine the microstructure and element composition. The crystal phase of the samples was identified by X-ray diffraction (XRD, Rigaku D/max) scanned at a scanning rate of 4 °/min using Cu Kα radiation. X-ray photoelectron spectroscopy (XPS, Thermo ESCALAB 250XI) can analyze the chemical bonds of samples. At room temperature, the hysteresis loop of Fe_3O_4/C nanocomposites was evaluated using a vibrating sample magnetometer (Quantum Design, PPMS-9). The as-prepared Fe_3O_4/C composites were compressed into a circle ring of 7 mm in diameter to form the test specimen to explore the absorption performance of electromagnetic waves. The EMW absorption property can be tested by an EMW absorption analyzer (Agilent, N5230A). The test data includes the dielectric constant's real and imaginary parts and magnetic conductivity.

3. Results and discussion

3.1. Characterization of Fe_3O_4-spinach biocarbon composite

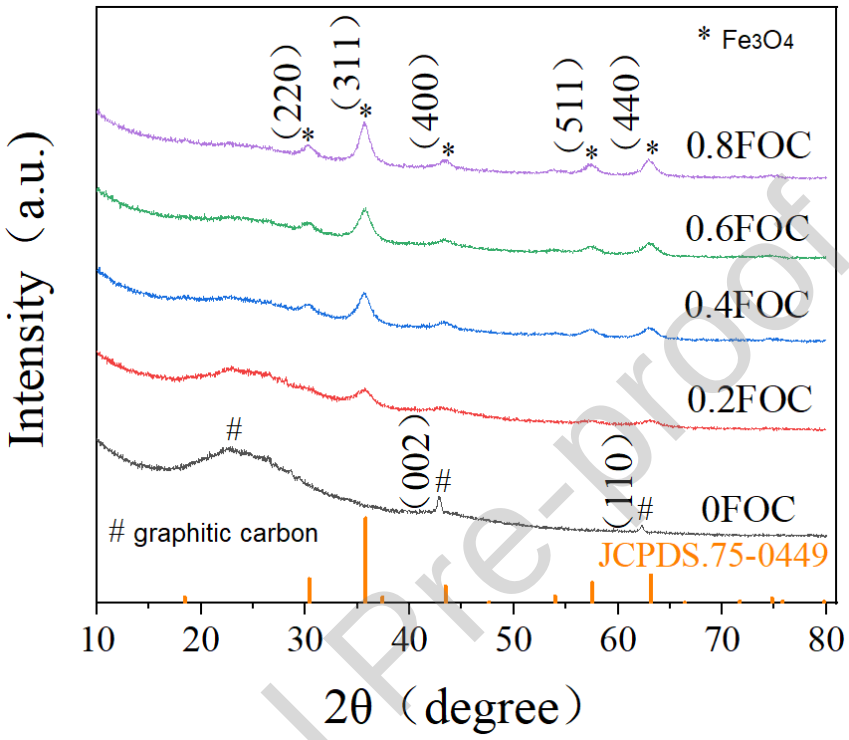

Fig. 1. XRD patterns of the xFOC samples.

The Fe_3O_4 decorated spinach-derived carbon composite (xFOC) phases composition and crystal structures were analyzed using XRD. In Fig. 1, the broad peak at 24.3° is graphite carbon, with a lattice plane of (002). While the low-intensity peaks at 43.0° and 62.5° indicate the (002) and (110) graphitic carbon crystal faces. The diffraction peaks of 0.4, 0.6 and 0.8FOC composites appearing at 30.2°, 35.6°, 43.2°, 57.2° and 62.7° are the crystal faces of Fe_3O_4, corresponding to the (220), (311), (400), (511) and (440) faces of Fe_3O_4 (JCPDS No. 75-0449), respectively [75]. In addition, the diffraction peaks at 30.2°, 43.2°, and 57.2° in the 0.2FOC sample are very weak, indicating that it has a relatively small content of Fe_3O_4 content, which may not be conducive to the absorption and consumption of electromagnetic waves. On the other hand, with the increasing Fe_3O_4 content, the characteristic peaks of graphite carbon are gradually weakened, even disappeared. This may mean that with the increase of Fe_3O_4 content, the strong Fe_3O_4 characteristic

peak gradually covers the characteristic peak of graphite carbon.

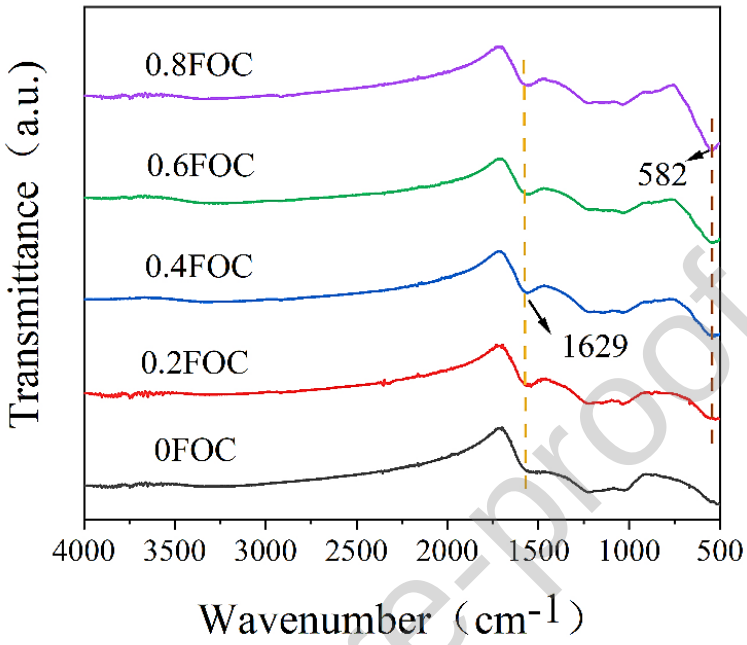

Fig. 2. The FTIR spectra of the xFOC samples.

The molecular characteristics of the sample were characterized by infrared spectroscopy. In Fig. 2, the 1629 cm^{-1} signal indicates the C=C bond tensile vibration derived from spinach stem carbon. Besides, the tensile vibration of Fe-O group shows a characteristic peak at 582 cm^{-1}, indicating the ferric oxide presence in the sample [82].

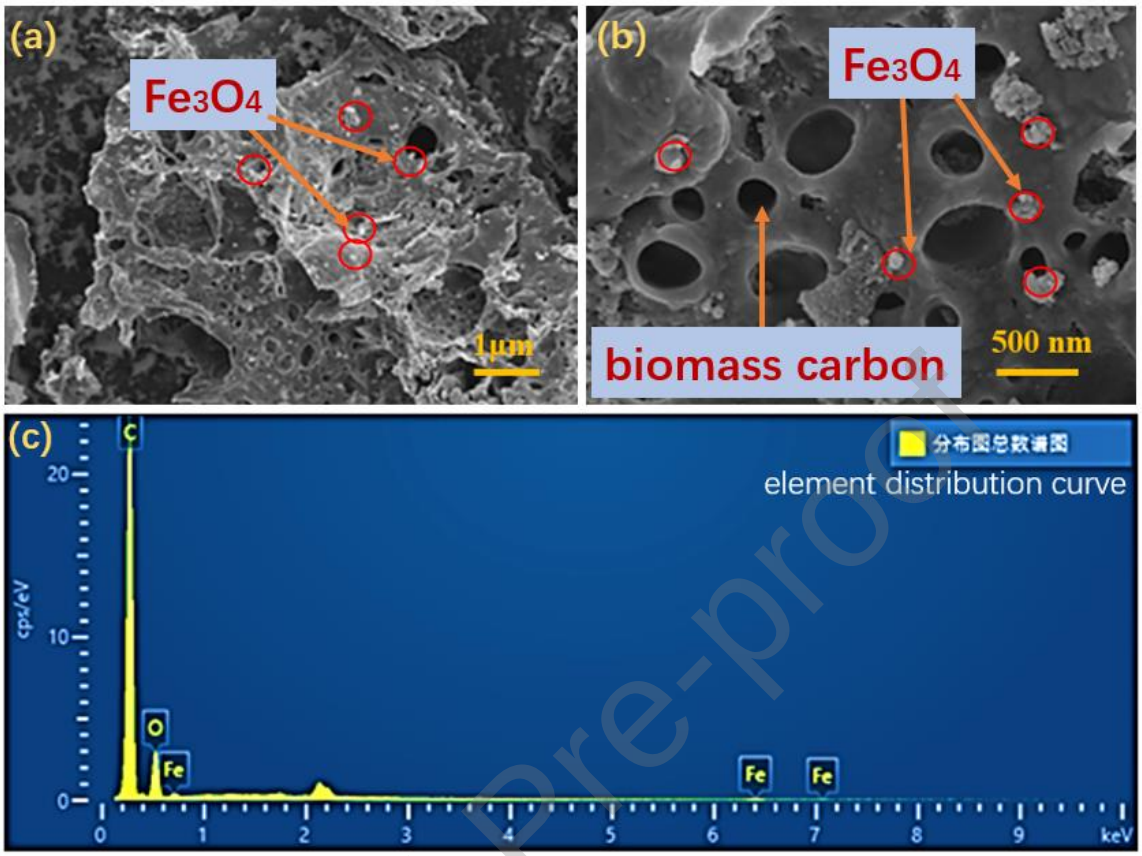

Fig. 3. SEM image of 0.4FOC, (a) 1 μm, (b) 500 nm, and (c) EDS.

Fig. 3 is the SEM-EDX test of the sample 0.4FOC. Fig. 3a shows a large number of open, well-developed porous structures in the sample. The size of these pores is approximately in the range of 200 - 500 nm. It can be seen that these porous structures penetrate the interior and surface of the bio-carbon. This can enable electromagnetic wave propagation and multiple reflections, thereby attenuating and absorbing electromagnetic waves. It can be seen from Fig. 3b that Fe_3O_4 nanoparticles take on an irregular shape, with a size of about 50-100 nm. These Fe_3O_4 nanoparticles may be easy to agglomerate after thermal drying. We can also see that Fe_3O_4 nanoparticles are located on the surface or filled in the internal pores of the bio-carbon. Fig. 3c depicts the EDS of the sample, which shows that the material is made up of carbon, iron, and oxygen, and the atomic percentages are 88.71%, 10.57%, and 0.72%, respectively.

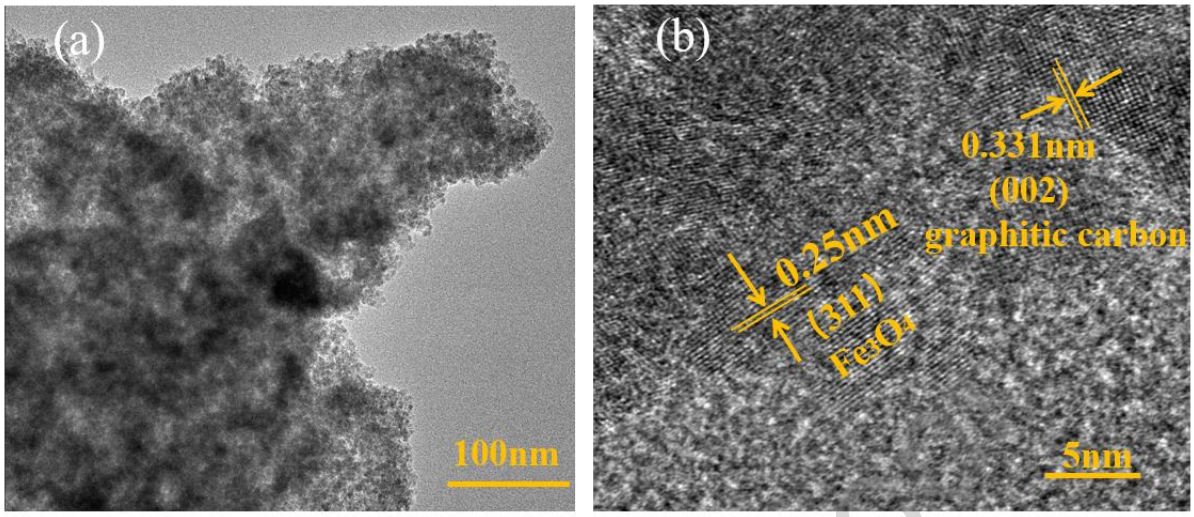

Fig. 4. (a) TEM image of 0.4FOC, (b) HRTEM image of 0.4FOC.

TEM can show the detailed morphologies of 0.4FOC sample. It can be observed from Fig. 4a that the Fe_3O_4 and bio-carbon are evenly distributed. Fig. 4b shows the HRTEM image showing the lattice pitch of around 0.331 nm, representing the (002) crystal face of graphitized carbon, while the crystal lattice fringe distance of 0.250 nm representing the (311) crystal surface of Fe_3O_4. These data are in agreement with the XRD results in Fig. 1 [82].

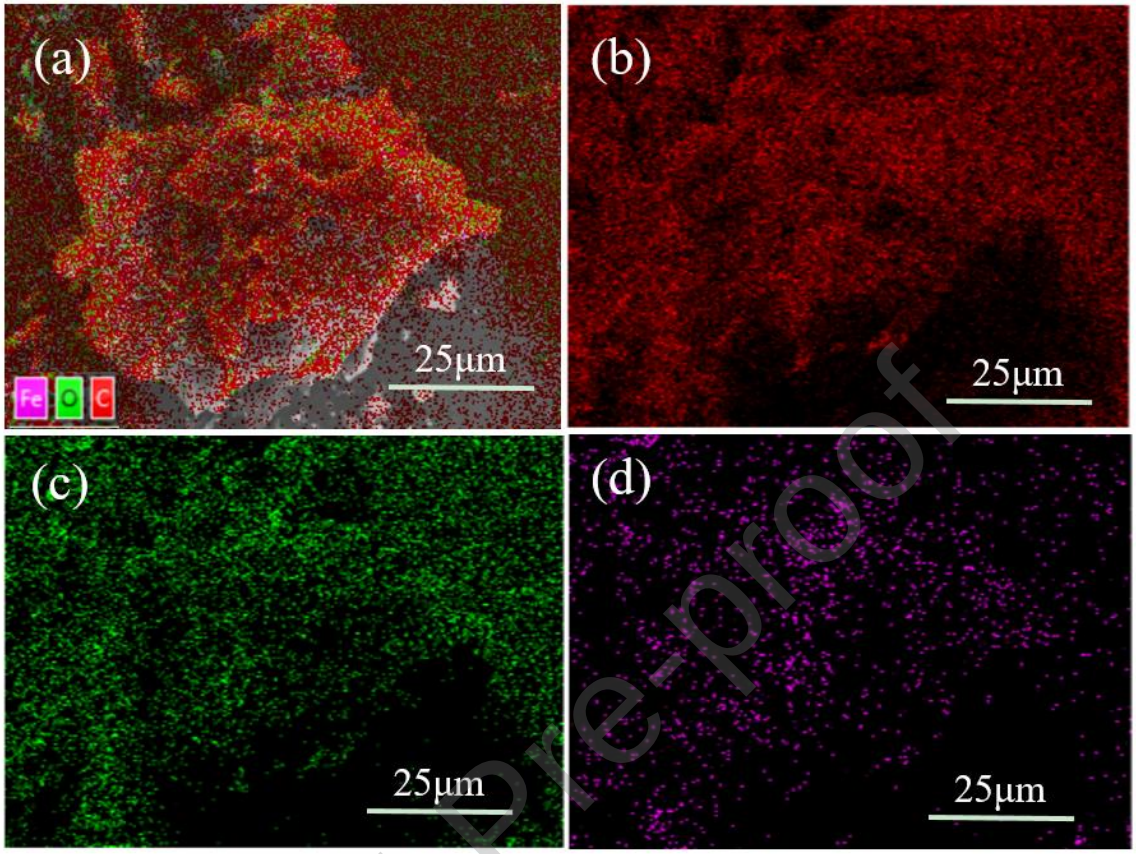

Fig. 5. Elemental mapping images of 0.4FOC (a), C (b), O (c), and Fe (d).Fig. 5 shows the elemental distribution of the sample 0.4FOC.

Fig. 5a shows the Fe_3O_4-bio-carbon composited particle, its size and morphology are also displayed in Fig. 3a-b. Fig. 5b-d are the distribution of C, O, and Fe elements in sample 0.4FOC, respectively. They are evenly distributed in the biological carbon matrix. The improvement in microwave absorption performance was due to the element's uniform dispersion [82]. The above XRD, SEM, TEM, and XPS tests showed consistent results, indicating that the Fe_3O_4-bio-carbon composite was successfully prepared.

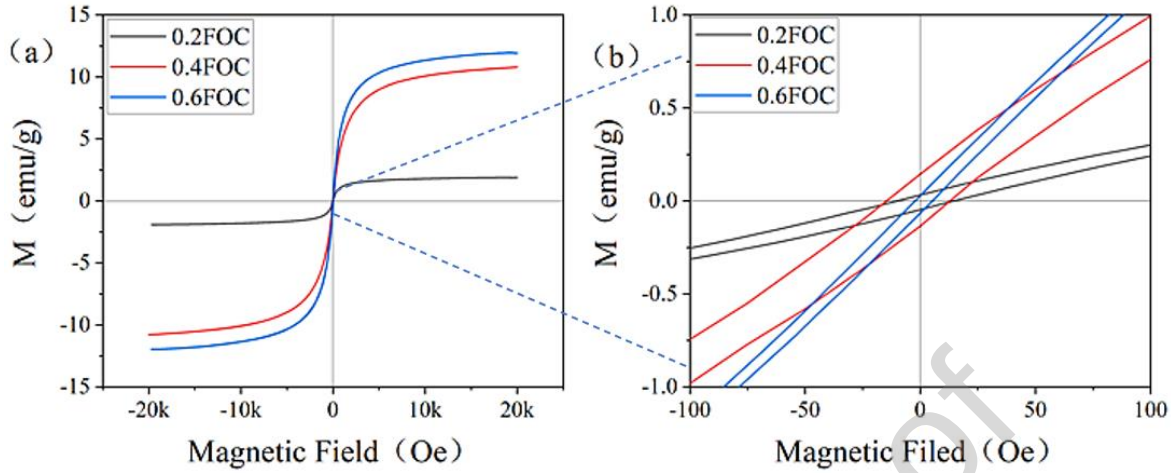

Fig. 6. The as-prepared samples magnetic hysteresis loops (a), (b) partially enlarged view of (a).

VSM tests the magnetic properties of FOC composite materials. As shown in Fig. 6a, the S-shaped hysteresis loop indicates that the sample has typical superparamagnetic characteristics. The magnetic properties of the samples are correlated with the content of the Fe_3O_4 in the samples and their magnetic conductivity. The saturation magnetization (M_s) of the three samples 0.2FOC, 0.4FOC, and 0.6FOC were 1.89, 10.75, and 11.95 emu/g, respectively. Fig. 6b shows the local amplification of Fig. 6a. As can be figured out, the coercivity (H_c) of the 0.4FOC sample is 29.36 Oe, and the remaining magnetization (M_r) is 0.28 emu/g, which is the largest in all the samples. It can be found from Fig. 6a and 6b that although sample 0.6FOC has more magnetic Fe_3O_4, the H_c and M_r of sample 0.4FOC were higher than those of sample 0.6FOC. These may have led to the result that 0.4FOC has a more superior electromagnetic wave absorption performance than other samples [83, 84].

3.2. Absorption performance and mechanism analysis

According to Maxwell's formula, the complex dielectric constant ($\varepsilon_r = \varepsilon' - j\varepsilon''$) and complex permeability ($\mu_r = \mu' - j\mu''$) are the two main arguments for electromagnetic wave absorption

properties. The real part (ε′) and imaginary part (ε″) of the dielectric constant in the parameters represent the storage capacity and loss volume of electrical energy, while the real part (μ′) and imaginary part (μ″) of the permeability reflecting the absorption and the ability to lose magnetic energy [85]. $\tan\delta_\varepsilon$ ($\tan\delta_\varepsilon = \varepsilon''/\varepsilon'$) and $\tan\delta_\mu$($\tan\delta_\mu = \mu''/\mu'$) are respectively called dielectric loss tangent and magnetic loss tangent. These two parameters can analyze the mechanism of composite materials absorbing electromagnetic microwaves [86].

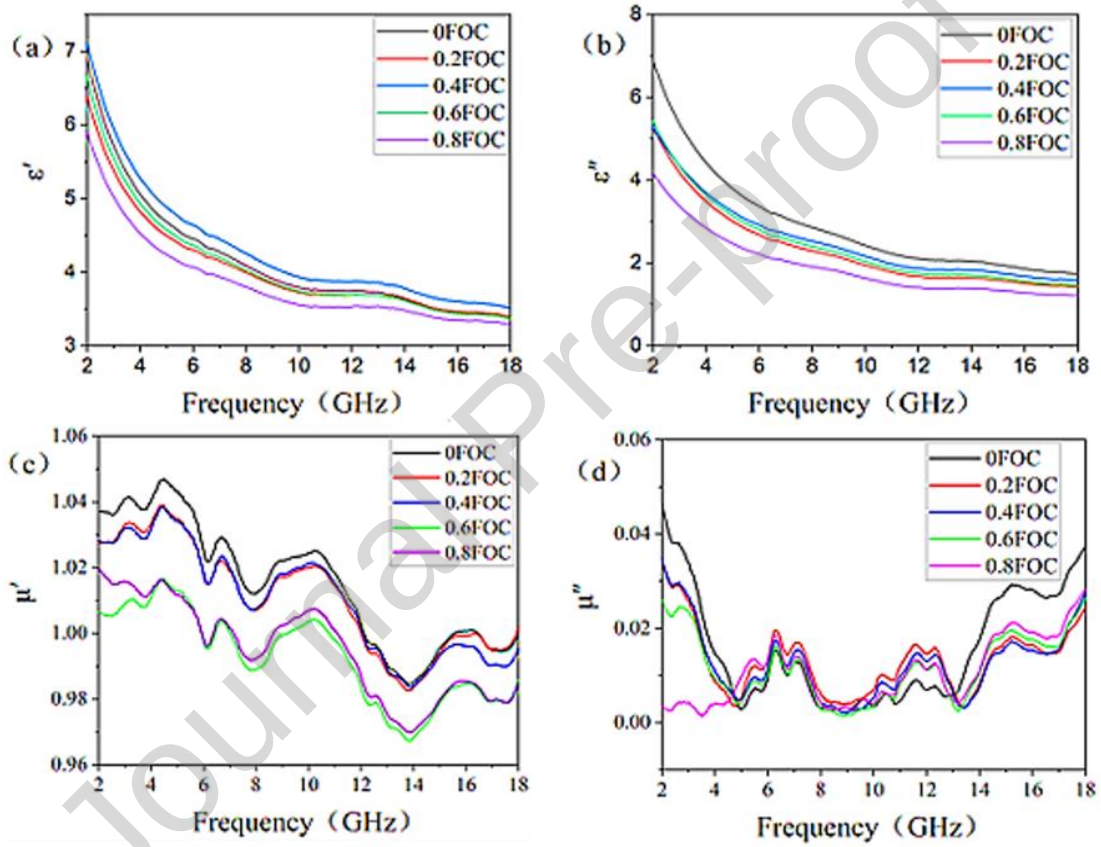

Fig. 7. Real (a) and imaginary (b) complex permittivity part of all samples, (c) real part, and (d) imaginary part of complex permeability of all samples.

As shown in Fig. 7a, the ε′ values of all samples show a downward trend as the frequency increases. This results from the delayed electric dipole orientation polarization compared to the periodic changes in the electric field [87]. In addition, the heterogeneous interface between Fe_3O_4 and spinage stem-derived bio-carbon blocks the movement of free electrons, resulting in a large number of electrons gathering at these junctions and an enhanced polarization of the interface. In other words, the combined dipole polarization effect and interface polarization reduce ε′.

According to the free-electron theory, dielectric losses include conductive and polarized relaxation losses. Therefore, conductive losses can reduce ε″. The occurrence of resonance peaks within the microwave range is due to polarization relaxation [88]. From the imaginary part of the permittivity in Fig. 7b, all samples ε′ values show a decreasing trend as the frequency increases. However, weak peaks within the 7-9 GHz range and 13-15 GHz indicate that the conductive loss decreases and the polarization relaxation loss increases. Among them, the ε″ value of 0FOC is the highest due to the inherent high dielectric properties of carbon materials. The dielectric properties decreased when the bio-carbon was composited with magnetic materials.

From the permeability of the real and imaginary parts in Fig. 7c and 7d, it can be observed that unlike the monotonic trend of ε′ and ε″, the curves of μ′ and μ″ have multiple strong vibration peaks. The magnetic energy storage capacity (μ′) and consumption capacity (μ″) can be significantly changed when the amount of Fe_3O_4 is different. When the Fe_3O_4 content in the samples increases, there are more resonance peaks in the μ′ and μ″ curves of all samples. Besides, multiple fluctuations can be observed in the low and high-frequency range. According to Aharoni's theory [89], natural resonance causes peaks in the low-frequency range. While the peaks in the high-frequency range originate from exchange resonance. This indicates that magnetic losses are the main factor in attenuating EMW absorption.

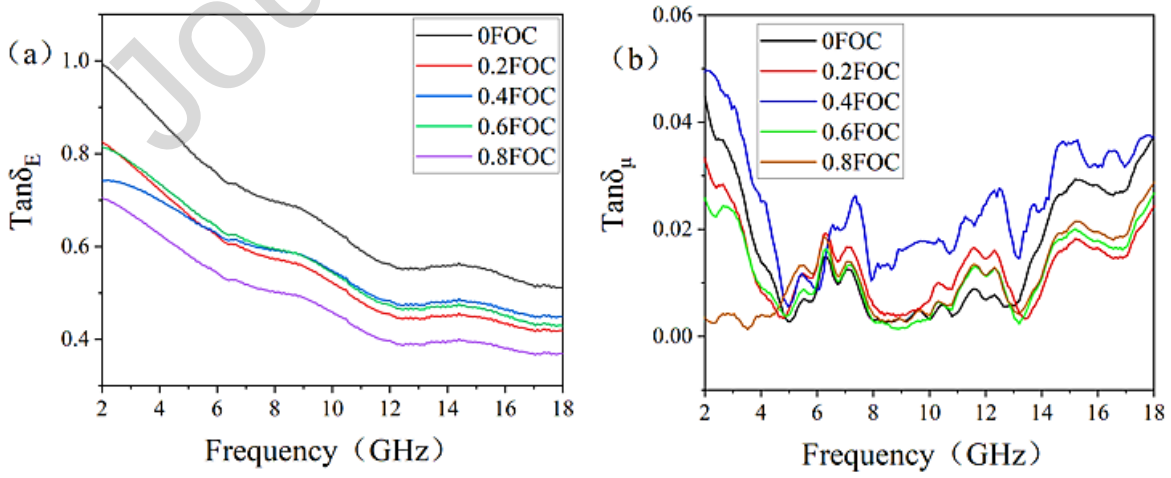

Fig. 8. The dielectric loss tangent (a) and magnetic loss tangent (b) of the as-prepared samples.

Fig. 8a shows that the dielectric loss of pure carbon materials is the largest because of the high dielectric properties of bio-carbon materials. The addition of magnetic materials will affect the dielectric loss coefficient of the material, but the dielectric loss of the sample 0.4FOC is greater than that of other samples. Fig. 8b depicts the magnetic loss tangent variation of the as-prepared samples. Among these, the magnetic loss coefficient of 0.4FOC is much larger than those of other samples. The results indicate that 0.4FOC has better dielectric and magnetic loss performance. Therefore, this sample plays a major role in the EMW absorption than other samples. All samples' dielectric loss and magnetic loss coefficients show that each sample's dielectric loss tangent value is much larger than the magnetic loss tangent value. These results also show that dielectric loss has a greater contribution to electromagnetic absorption than magnetic loss.

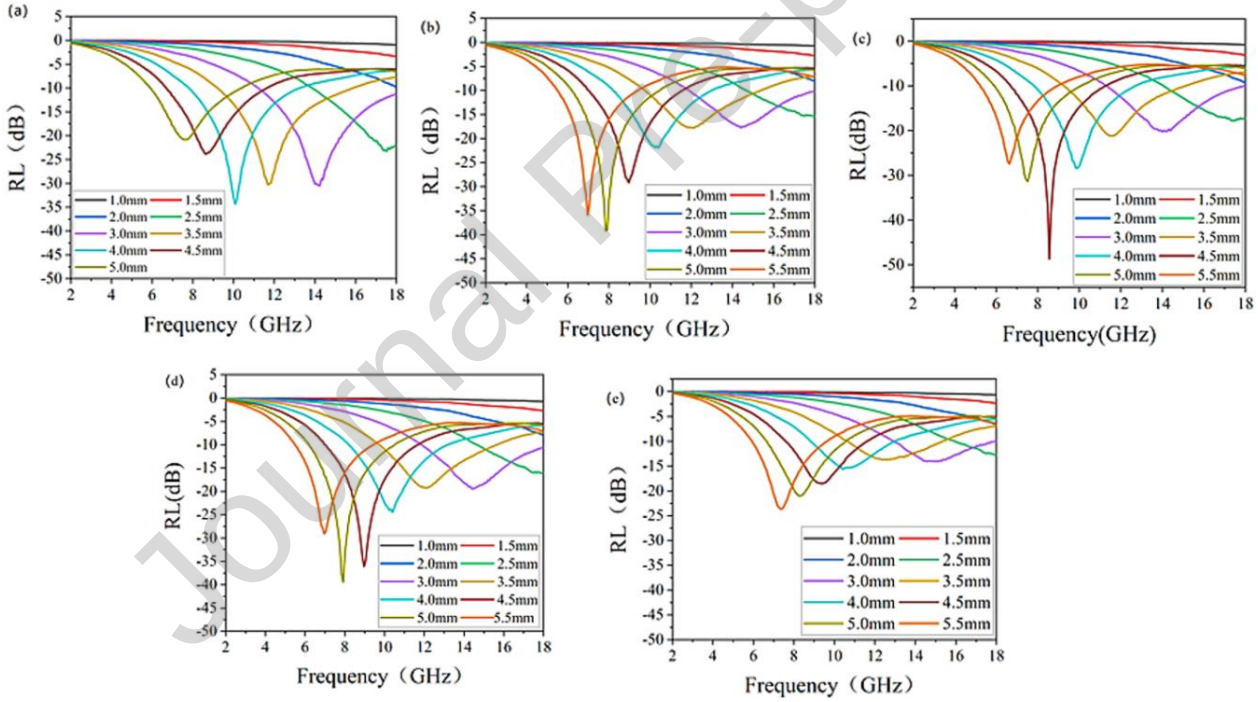

Fig. 9. Frequency dependence of RL values at different matching thicknesses, (a) 0FOC, (b) 0.2FOC, (c) 0.4FOC, (d) 0.6FOC and (e) 0.8FOC.

The RL value is important to evaluate the electromagnetic wave absorption performance of a material. According to the transmission line theory, it can be inferred that at different frequencies and material thicknesses of samples, the reflection loss is related to the complex dielectric constant and complex magnetic permeability as follows [90]:

$$RL(dB) = 20\log|(Z_{in} - Z_0)/(Z_{in} + Z_0)| \quad (1)$$

$$Z_{in} = Z_0\sqrt{\frac{\mu_r}{\varepsilon_r}}\tan h\left(j\frac{2\pi fd}{c}\sqrt{\mu_r\varepsilon_r}\right) \quad (2)$$

where Z_0 and Z_{in} refer to the input resistance of the free space and the wave-absorbing material separately. Therein, μ_γ is the complex permeability. ε_γ is the complex dielectric constant. *f* refers to the electromagnetic wave frequency. d stands for the thickness. c is the velocity of light in empty space. When the RL value is below -10dB, it shows that over 90% of the electromagnetic wave can be completely absorbed, and this absorption frequency range can be considered an effective absorption band [91].

As the reflection loss shown in Fig. 9a-e, the minimum RL value corresponding to samples 0FOC, 0.2FOC, 0.4FOC, 0.6FOC, and 0.8FOC are -33.59 dB, -38.87 dB, -48.81 dB, -39.45 dB and -23.73 dB, respectively when the frequency is 10.06 GHz. When the absorbing material is only 3.5mm thick, the minimum RL value corresponding to 0.4FOC at 8.51GHz is about -48.81 dB, and the effective absorption bandwidth reaches 4.73 GHz. 0.4FOC sample has the best microwave absorption performance of all the tested samples. This may be the most appropriate bio-carbon to Fe_3O_4 ratio in 0.4FOC. As to 0FOC, the high dielectric loss of pure carbon makes its minimum RL value -38.87 dB. As to the samples of 0.6FOC and 0.8FOC, its microwave absorption performance is affected due to the relatively high Fe_3O_4 content. When the amount of biocarbon in the samples increases, the porosity increases. However, this does not mean an enhanced wave absorption performance. It is also very important that a good impedance matching is needed with suitable amount of Fe_3O_4 in the sample. Generally, an ideal absorbing material is believed to have strong electromagnetic wave absorption strength, a broad absorption frequency spectrum, lightness, thinness, and low density. The 0.4FOC sample showed good above-mentioned comprehensive characteristics, indicating that it has good electromagnetic wave absorption and attenuation performance.

In addition, as the thickness of all samples increases, the absorption peaks shift towards the low-frequency region. The following quarter-wavelength (l/4) matching model can be used to

explain the phenomenon [92]:

$$t_m = \frac{nc}{4f_m\sqrt{|\mu r||\varepsilon r|}} \quad (n = 1,\ 3,\ 5\cdots) \qquad (3)$$

where t_m represents the thickness under the minimum reflection loss of the matching and f_m the frequency corresponding to the RL_{min} peak under the matching thickness.

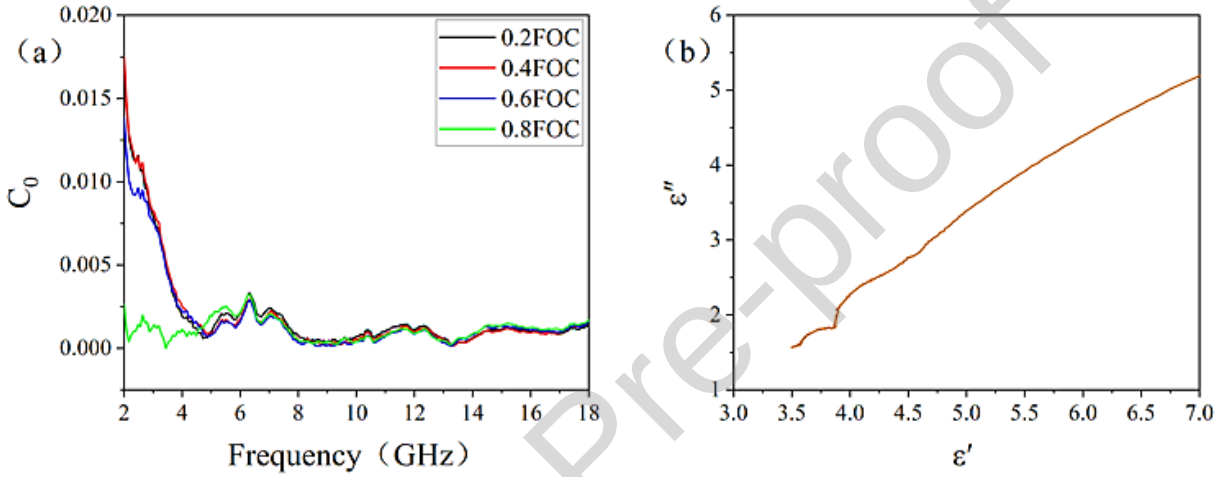

Fig. 10. (a) C_0 curves of the as-prepared samples, (b) Typical Cole-Cole semicircles for the sample 0.4FOC.

Generally, the magnetic losses at the frequency of GHz include eddy losses, natural syntony losses, and exchange syntony losses. Among them, we can give the data of eddy current losses by using the formula (4):

$$C_0 = \mu''(\mu')^{-2}f^{-1} \qquad (4)$$

If eddy loss is the main source of magnetic loss, C_0 does not fluctuate with frequency. As shown in Fig. 10a, except for the 0.8FOC sample, the C_0 of all other samples dropped rapidly in the low-frequency range and gradually approached certain values. This evidences that the magnetic loss at high frequency originates from the eddy loss, which is connected with the relatively high conductivity of composite materials [93].

Debye dielectric relaxation model can calculate the dielectric losses of this wave-absorbing material. Therefore, the relative complex permittivity is given by:

$$\varepsilon' = \varepsilon_\infty + \frac{\varepsilon_s - \varepsilon_\infty}{1+\omega^2\tau^2} \quad (5)$$

$$\varepsilon'' = \frac{\varepsilon_s - \varepsilon_\infty}{1+\omega^2\tau^2}\omega\tau + \frac{\sigma}{\omega\varepsilon_0} \quad (6)$$

According to the above two formulas, the relation between ε' and ε" can be deduced as:

$$\left(\varepsilon' - \frac{\varepsilon_s + \varepsilon_\infty}{2}\right)^2 + (\varepsilon'')^2 = \left(\frac{\varepsilon_s - \varepsilon_\infty}{2}\right)^2 \quad (7)$$

As a result, the graph of ε′ and ε″ will be a separate semicircle. It is generally called a cole-Cole semicircle. Every semicircle represents a Debye relaxation process. It is possible that sometimes there is a complex polarization process during electromagnetic wave absorption. In this case, the Cole semicircle is distorted and consists of more than one semicircle [94].

The ε′-ε″ curve of 0.4FOC composite is shown in Fig. 10b. There are two semicircles, and a tail can be found in the figure. Therein, the former semicircle is related to the multi-polarization relaxation process. However, the latter referred to the conductivity loss [95]. In general, the polarization effect can be specifically manifested as “interface polarization, dipole polarization, ion polarization, and electron polarization [96]. Classically, electron and ion polarization often occur in the region of from103 to 106 GHz [97, 98]. At the same time, the dipole and interface polarization occur within from 2 to 18 GHz. Therefore, it can be explained that the as-prepared xFOC materials absorb electromagnetic waves by the combined polarization relaxation and conductivity losses.

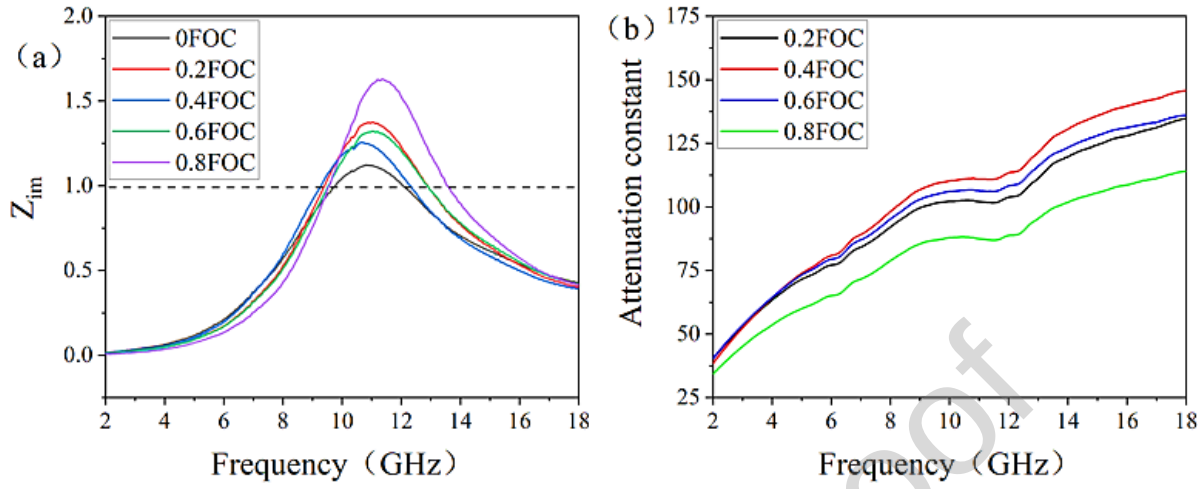

Fig. 11. Impedance matching (a) and attenuation coefficient (b) of xFOC composite samples.

Generally, magnetic Fe_3O_4 introduction into carbon material will make the impedance matching (Z_{im}) closer to 1. When Z_{im} has a value equal to 1, it means a perfect impedance matching. From the impedance matching diagram in Fig. 11a, we know that Z_{im} value of 0.6FOC in the frequency range of 9.7-12.1 GHz reaches a maximum of about 1.1. The Z_{im} value of 0.4FOC in the 9.18-12.35 GHz range is about 1.25. The maximum values of other samples were about 1.36 and 1.61, respectively. As a result, the electromagnetic wave absorption performance is determined by the combined effects of dielectric loss, magnetic loss, and impedance matching. The attenuation loss in Fig. 11b shows that the attenuation constant value of 0.4FOC is significantly larger than other samples, especially when the frequency exceeds 5.2GHz. This means that the sample 0.4FOC has better microwave absorption and attenuation performance.

4. Conclusions

In this work, magnetic Fe_3O_4 decorated spinach-derived carbon composites were successfully prepared through a hydrothermal-calcination process. The as prepared microwave absorbing material is characterized by its light weight and good electromagnetic wave absorption performance. At the matching thickness of 4.5 mm, the optimal raw material ratio sample 0.4FOC has a minimal RL value of -48.81dB and a bandwidth of 4.77 GHz. In addition, the filling rate is only 15%. The mechanism testing and analysis show that the enhanced electromagnetic wave

absorption performance is the result of a combination of dielectric loss, magnetic loss, numerous reflections, and efficient impedance matching. Although we have not done the big batch experiment, and do not know if there will be obvious difference. The above figures and data have shown a very good stability and replicability. Therefore, believe that the as-prepared composite of Fe_3O_4 with spinach-derived bio-carbon will have good application prospects.

Declaration of Competing Interest

The authors declare that they have no known competitive economic interests or personal relationships that may affect the work reported in this article.

Acknowledgments

This work has been supported by the Innovation and Entrepreneurship Training Program for Chinese College Students. We are also very grateful for the testing equipment and techniques provided by Beijing Aerospace Research Institute of Materials and Processing Technology. The authors extend their appreciation to Taif University, Saudi Arabia for supporting this work through project number (TU-DSPP-2024-03).

References

[1] R. Dilli, R. Ch, r.M. L , D. Jordhana, Ultra-Massive Multiple Input Multiple Output Technologies for 6G Wireless Networks, Engineered Science 16 (2021) 308-318.
[2] J. Cao, H. Yao, Y. Pang, J. Xu, C. Lan, M. Lei, K. Bi, Dual-band piezoelectric artificial structure for very low frequency mechanical antenna, Advanced Composites and Hybrid Materials 5(1) (2022) 410-418.
[3] T. Li, H. Wei, Y. Zhang, T. Wan, D. Cui, S. Zhao, T. Zhang, Y. Ji, H. Algadi, Z. Guo, L. Chu, B. Cheng, Sodium alginate reinforced polyacrylamide/xanthan gum double network ionic hydrogels for stress sensing and self-powered wearable device applications, Carbohydrate Polymers 309 (2023) 120678.
[4] G. Zhao, F. Qian, X. Li, Y. Tang, Y. Sheng, H. Li, J. Rao, M.V. Singh, H. Algadi, M. Niu, W. Zhang, Z. Guo, X. Peng, T. Chen, Constructing a continuous reduced graphene oxide network in porous plant fiber sponge for highly compressible and sensitive piezoresistive sensors, Advanced Composites and Hybrid Materials 6(5) (2023) 184.
[5] V.K. Shukla, M. Sudhi, D.K. Shetty, S. Banthia, P. Chandrasekar, N. Naik, B.M.Z. Hameed, G. S, J.M. Balakrishnan, Transforming Disease Diagnosis and Management: A Comprehensive

Review of AI-Driven Urine Analysis in Clinical Medicine, Engineered Science 26 (2023) 1009.
[6] S.A. Al-Zhrani, N.M. Bedaiwi, I.F.E. El-Ramli, A.Z. Barasheed, A. Abduldaiem, Y.A. Al-Hadeethi , A. Umar, Underwater Optical Communications: A Brief Overview and Recent Developments, Engineered Science 16 (2021) 146–186.
[7] Q. Jiang, Y. Qiao, C. Xiang, A. Uddin, L. Wu, F. Qin, Metacomposite based on three-dimensional ferromagnetic microwire architecture for electromagnetic response, Advanced Composites and Hybrid Materials 5(4) (2022) 3190-3200.
[8] X.-Y. Ye, Y. Chen, J. Yang, H.-Y. Yang, D.-W. Wang, B.B. Xu, J. Ren, D. Sridhar, Z. Guo, Z.-J. Shi, Sustainable wearable infrared shielding bamboo fiber fabrics loaded with antimony doped tin oxide/silver binary nanoparticles, Advanced Composites and Hybrid Materials 6(3) (2023) 106.
[9] Y. Duan, Z. Xiao, X. Yan, Z. Gao, Y. Tang, L. Hou, Q. Li, G. Ning, Y. Li, Enhanced Electromagnetic Microwave Absorption Property of Peapod-like MnO@carbon Nanowires, ACS Applied Materials & Interfaces 10(46) (2018) 40078-40087.
[10] J. Ruan, Z. Chang, H. Rong, T.S. Alomar, D. Zhu, N. AlMasoud, Y. Liao, R. Zhao, X. Zhao, Y. Li, B.B. Xu, Z. Guo, Z.M. El-Bahy, H. Li, X. Zhang, S. Ge, High-conductivity nickel shells encapsulated wood-derived porous carbon for improved electromagnetic interference shielding, Carbon 213 (2023) 118208.
[11] H. Cheng, L. Xing, Y. Zuo, Y. Pan, M. Huang, A. Alhadhrami, M.M. Ibrahim, Z.M. El-Bahy, C. Liu, C. Shen, X. Liu, Constructing nickel chain/MXene networks in melamine foam towards phase change materials for thermal energy management and absorption-dominated electromagnetic interference shielding, Advanced Composites and Hybrid Materials 5(2) (2022) 755-765.
[12] X. Wang, C. Li, H. Geng, J. Xie, Z. Chen, X. Zhang, C. Xiong, S. Wang, Tunable dielectric properties and electromagnetic wave absorbing performance of MoS_2/Fe_3O_4/PANI composite, Colloids and Surfaces A: Physicochemical and Engineering Aspects 637 (2022) 128285.
[13] X. Chai, D. Zhu, Q. Chen, Y. Qing, K. Cao, F. Luo, Z. Huang, P. Li, X. Liu, Tailored composition of low emissivity top layer for lightweight visible light-infrared-radar multiband compatible stealth coating, Advanced Composites and Hybrid Materials 5(4) (2022) 3094-3103.
[14] Z. Qu, J. Hao, H. Jing, Y. Wei, J. Duan, J. Wang, B. Zhang, An ultra-thin ultra-broadband microwave absorber for radar stealth, Advanced Composites and Hybrid Materials 5(3) (2022) 1778-1785.
[15] W. Wang, D. Liu, H. Cheng, T. Cao, Y. Li, Y. Deng, W. Xie, Structural design and broadband radar absorbing performance of multi-layer patch using carbon black, Advanced Composites and Hybrid Materials 5(4) (2022) 3137-3145.
[16] B. Dai, Y. Ma, F. Dong, J. Yu, M. Ma, H.K. Thabet, S.M. El-Bahy, M.M. Ibrahim, M. Huang, I. Seok, G. Roymahapatra, N. Naik, B.B. Xu, J. Ding, T. Li, Overview of MXene and conducting polymer matrix composites for electromagnetic wave absorption, Advanced Composites and Hybrid Materials 5(2) (2022) 704-754.
[17] S. Zhang, B. Cheng, Z. Jia, Z. Zhao, X. Jin, Z. Zhao, G. Wu, The art of framework construction: hollow-structured materials toward high-efficiency electromagnetic wave absorption, Advanced Composites and Hybrid Materials 5(3) (2022) 1658-1698.

[18] Y. Long, Z. Zhang, K. Sun, C. Wang, N. Zeng, B. Gao, X. Tang, X. Qi, R. Fan, Enhanced electromagnetic wave absorption performance of hematite@carbon nanotubes/polyacrylamide hydrogel composites with good flexibility and biocompatibility, Advanced Composites and Hybrid Materials 6(5) (2023) 173.
[19] T. Zhao, X. Ji, W. Jin, C. Wang, W. Ma, J. Gao, A. Dang, T. Li, S. Shang, Z. Zhou, Direct in situ synthesis of a 3D interlinked amorphous carbon nanotube/graphene/BaFe12O19 composite and its electromagnetic wave absorbing properties, RSC Advances 7(26) (2017) 15903-15910.
[20] S. Zhang, Z. Jia, B. Cheng, Z. Zhao, F. Lu, G. Wu, Recent progress of perovskite oxides and their hybrids for electromagnetic wave absorption: a mini-review, Advanced Composites and Hybrid Materials 5(3) (2022) 2440-2460.
[21] Y. Sun, N. Wang, H. Yu, X. Jiang, Metal–organic framework-based Fe/C@Co3O4 core–shell nanocomposites with outstanding microwave absorption properties in low frequencies, Journal of Materials Science 55(17) (2020) 7304-7320.
[22] F. Li, N. Wu, H. Kimura, Y. Wang, B.B. Xu, D. Wang, Y. Li, H. Algadi, Z. Guo, W. Du, C. Hou, Initiating Binary Metal Oxides Microcubes Electromagnetic Wave Absorber Toward Ultrabroad Absorption Bandwidth Through Interfacial and Defects Modulation, Nano-Micro Letters 15(1) (2023) 220.
[23] C. Wang, H. Gao, D. Liang, S. Liu, H. Zhang, H. Guan, Y. Wu, Y. Zhang, Effective fabrication of flexible nickel chains/acrylate composite pressure-sensitive adhesives with layered structure for tunable electromagnetic interference shielding, Advanced Composites and Hybrid Materials 5(4) (2022) 2906-2920.
[24] Z. Zhang, Z. Li, Y. Zhao, X. Bi, Z. Zhang, Z. Long, Z. Liu, L. Zhang, W. Cai, Y. Liu, R. Fan, Dielectric enhancement effect in biomorphic porous carbon-based iron@iron carbide 'meta-powder' for light-weight microwave absorption material design, Advanced Composites and Hybrid Materials 5(4) (2022) 3176-3189.
[25] H. Wang, D. Zhu, W. Zhou, F. Luo, Effect of Multiwalled Carbon Nanotubes on the Electromagnetic Interference Shielding Properties of Polyimide/Carbonyl Iron Composites, Industrial & Engineering Chemistry Research 54(25) (2015) 6589-6595.
[26] Y. Shu, T. Zhao, X. Li, a. Jalil, L. Yang, G. Feng, Y. Li, W. Jia, F. Luo, Enhancing electromagnetic wave absorption and hydrophobicity/heat insulation properties of coral-like Co/CoO/RGO aerogels through pore structure regulation, Carbon 213 (2023) 118278.
[27] G. Cao, S. Cai, H. Zhang, Y. Tian, High-performance conductive adhesives based on water-soluble resins for printed circuits, flexible conductive films, and electromagnetic interference shielding devices, Advanced Composites and Hybrid Materials 5(3) (2022) 1730-1742.
[28] J. Guo, Z. Chen, X. Xu, X. Li, H. Liu, S. Xi, W. Abdul, Q. Wu, P. Zhang, B.B. Xu, J. Zhu, Z. Guo, Enhanced electromagnetic wave absorption of engineered epoxy nanocomposites with the assistance of polyaniline fillers, Advanced Composites and Hybrid Materials 5(3) (2022) 1769-1777.
[29] D. Lan, Y. Wang, Y. Wang, X. Zhu, H. Li, X. Guo, J. Ren, Z. Guo, G. Wu, Impact mechanisms of aggregation state regulation strategies on the microwave absorption properties of flexible polyaniline, Journal of Colloid and Interface Science 651 (2023) 494-503.

[30] K. Liu, W. Liu, W. Li, Y. Duan, K. Zhou, S. Zhang, S. Ni, T. Xu, H. Du, C. Si, Strong and highly conductive cellulose nanofibril/silver nanowires nanopaper for high performance electromagnetic interference shielding, Advanced Composites and Hybrid Materials 5(2) (2022) 1078-1089.
[31] M. Seol, U. Hwang, J. Kim, D. Eom, I.-K. Park, H. Kim, J. Suhr, J.-D. Nam, Solution printable multifunctional polymer-based composites for smart electromagnetic interference shielding with tunable frequency and on–off selectivities, Advanced Composites and Hybrid Materials 6(1) (2023) 46.
[32] C. Wu, L. Zeng, G. Chang, Y. Zhou, K. Yan, L. Xie, B. Xue, Q. Zheng, Composite phase change materials embedded into cellulose/polyacrylamide/graphene nanosheets/silver nanowire hybrid aerogels simultaneously with effective thermal management and anisotropic electromagnetic interference shielding, Advanced Composites and Hybrid Materials 6(1) (2023) 31.
[33] N. Wu, B. Zhao, X. Chen, C. Hou, M. Huang, A. Alhadhrami, G.A.M. Mersal, M.M. Ibrahim, J. Tian, Dielectric properties and electromagnetic simulation of molybdenum disulfide and ferric oxide-modified Ti3C2TX MXene hetero-structure for potential microwave absorption, Advanced Composites and Hybrid Materials 5(2) (2022) 1548-1556.
[34] B. Miao, Y. Cao, Q. Zhu, M.A. Nawaz, J.A. Ordiozola, T.R. Reina, Z. Bai, J. Ren, F. Wei, Scalable synthesis of 2D Ti2CTx MXene and molybdenum disulfide composites with excellent microwave absorbing performance, Advanced Composites and Hybrid Materials 6(2) (2023) 61.
[35] L. She, B. Zhao, M. Yuan, J. Chen, B. Fan, H. Pan, R. Che, Joule-heated flexible carbon composite towards the boosted electromagnetic wave shielding properties, Advanced Composites and Hybrid Materials 5(4) (2022) 3012-3022.
[36] H. Zhao, Y. Cheng, J. Ma, Y. Zhang, G. Ji, Y. Du, A sustainable route from biomass cotton to construct lightweight and high-performance microwave absorber, Chemical Engineering Journal 339 (2018) 432-441.
[37] Y. Huang, S. Chen, R. Ma, Y. Cheng, L. Jin, G. Chen, Coal-based carbon composite with excellent electromagnetic-shielding properties prepared from modification of coal with D-A reaction, Advanced Composites and Hybrid Materials 5(3) (2022) 2193-2205.
[38] H. Du, J. Jiang, L. Ren, Q. He, Y. Wang, Fe_3C/Fe@N-doped porous carbon composites with excellent microwave absorption properties, Colloids and Surfaces A: Physicochemical and Engineering Aspects 670 (2023) 131564.
[39] F. Li, Q. Li, H. Kimura, X. Xie, X. Zhang, N. Wu, X. Sun, B.B. Xu, H. Algadi, R.A. Pashameah, A.K. Alanazi, E. Alzahrani, H. Li, W. Du, Z. Guo, C. Hou, Morphology controllable urchin-shaped bimetallic nickel-cobalt oxide/carbon composites with enhanced electromagnetic wave absorption performance, Journal of Materials Science & Technology 148 (2023) 250-259.
[40] H. Wang, D. Zhu, W. Zhou, F. Luo, Temperature dependence of the electromagnetic and microwave absorption properties of polyimide/Ti3SiC2 composites in the X band, RSC Advances 5(105) (2015) 86656-86664.
[41] P. Wang, L. Cheng, L. Zhang, One-dimensional carbon/SiC nanocomposites with tunable dielectric and broadband electromagnetic wave absorption properties, Carbon 125 (2017) 207-220.

[42] C. Wei, L. Shi, M. Li, M. He, M. Li, X. Jing, P. Liu, J. Gu, Hollow engineering of sandwich NC@Co/NC@MnO2 composites toward strong wideband electromagnetic wave attenuation, Journal of Materials Science & Technology 175 (2024) 194-203.
[43] T. Zhao, W. Jin, X. Ji, J. Gao, C. Xiong, A. Dang, H. Li, T. Li, S. Shang, Z. Zhou, Preparation and electromagnetic wave absorbing properties of 3D graphene/pine needle-like iron nano-acicular whisker composites, RSC Advances 7(26) (2017) 16196-16203.
[44] X. Lu, D. Zhu, X. Li, Y. Wang, Architectural design and interfacial engineering of CNTs@ZnIn2S4 heterostructure/cellulose aerogel for efficient electromagnetic wave absorption, Carbon 197 (2022) 209-217.
[45] B. Wang, Q. Wu, Y. Fu, T. Liu, A review on carbon/magnetic metal composites for microwave absorption, Journal of Materials Science & Technology 86 (2021) 91-109.
[46] X. Liu, H. Xu, F. Xie, C. Fasel, X. Yin, R. Riedel, Highly flexible and ultrathin Mo2C film via in-situ growth on graphene oxide for electromagnetic shielding application, Carbon 163 (2020) 254-264.
[47] L. Yan, W. Jiang, C. Zhang, Y. Zhang, Z. He, K. Zhu, N. Chen, W. Zhang, B. Han, X. Zheng, Enhancement by Metallic Tube Filling of the Mechanical Properties of Electromagnetic Wave Absorbent Polymethacrylimide Foam, Polymers 11(2) (2019) 372.
[48] Z. Wu, K. Tian, T. Huang, W. Hu, F. Xie, J. Wang, M. Su, L. Li, Hierarchically Porous Carbons Derived from Biomasses with Excellent Microwave Absorption Performance, ACS Applied Materials & Interfaces 10(13) (2018) 11108-11115.
[49] Z. Jia, X. Zhang, Z. Gu, G. Wu, MOF-derived Ni-Co bimetal/porous carbon composites as electromagnetic wave absorber, Advanced Composites and Hybrid Materials 6(1) (2023) 28.
[50] C. Chen, J. Xi, Y. Han, L. Peng, W. Gao, Z. Xu, C. Gao, Ultralight graphene micro-popcorns for multifunctional composite applications, Carbon 139 (2018) 545-555.
[51] X. Zhu, Z. Wang, J. Ren, N. AlMasoud, Z.M. El-Bahy, T. S.Alomar, C. Zhang, J. Zhang, J. Zhou, M. Li, D. Wang, I. Seok, X. Guo, Graphene/polyacrylamide interpenetrating structure hydrogels for wastewater treatment, Advanced Composites and Hybrid Materials 6(5) (2023) 169.
[52] Z. Cui, J. Zhou, X. Wang, Q. Wang, J. Si, X. Liu, In situ growth of bimetallic nickel cobalt sulfide ($NiCo_2S_4$) nanowire arrays encapsulated by nitrogen-doped carbon on carbon cloth as binder-free and flexible electrode for high-performance aqueous Zn batteries, Advanced Composites and Hybrid Materials 6(3) (2023) 95.
[53] X. Yan, Y. Tu, H. Yuan, Y. Xia, Y. Jiang, S. Zhu, C. Li, H. Tang, P. Du, M. Lei, Experimental and theoretical insights into cobalt nanoparticles encapsulated in N- and S-codoped carbon as advanced bifunctional electrocatalyst for rechargeable zinc-air batteries, Advanced Composites and Hybrid Materials 6(2) (2023) 71.
[54] G. Yuan, T. Wan, A. BaQais, Y. Mu, D. Cui, M.A. Amin, X. Li, B.B. Xu, X. Zhu, H. Algadi, H. Li, P. Wasnik, N. Lu, Z. Guo, H. Wei, B. Cheng, Boron and fluorine Co-doped laser-induced graphene towards high-performance micro-supercapacitors, Carbon 212 (2023) 118101.
[55] M. Kumari, G.R. Chaudhary, S. Chaudhary , A. Umar, Rapid Analysis of Trace Sulphite Ion Using Fluorescent Carbon Dots Produced from Single Use Plastic Cups, Engineered Science 17 (2022) 101-112.

[56] S. Abazari, A. Shamsipur, H.R. Bakhsheshi-Rad, A.F. Ismail, S. Sharif, M. Razzaghi, S. Ramakrishna, F. Berto, Carbon Nanotubes (CNTs)-Reinforced Magnesium-Based Matrix Composites: A Comprehensive Review, Materials 13(19) (2020) 4421.
[57] S. Abazari, A. Shamsipur, H.R. Bakhsheshi-Rad, S. Ramakrishna, F. Berto, Graphene Family Nanomaterial Reinforced Magnesium-Based Matrix Composites for Biomedical Application: A Comprehensive Review, Metals 10(8) (2020) 1002.
[58] A. Nazir, H. Yu, L. Wang, M. Haroon, R.S. Ullah, S. Fahad, K.-u.-R. Naveed, T. Elshaarani, A. Khan, M. Usman, Recent progress in the modification of carbon materials and their application in composites for electromagnetic interference shielding, Journal of Materials Science 53(12) (2018) 8699-8719.
[59] P. Chen, L.-K. Wang, G. Wang, M.-R. Gao, J. Ge, W.-J. Yuan, Y.-H. Shen, A.-J. Xie, S.-H. Yu, Nitrogen-doped nanoporous carbon nanosheets derived from plant biomass: an efficient catalyst for oxygen reduction reaction, Energy & Environmental Science 7(12) (2014) 4095-4103.
[60] B. Yuan, Y. Wang, A.Y. Elnaggar, I.H.E. Azab, M. Huang, M.H.H. Mahmoud, S.M. El-Bahy, M. Guo, Physical vapor deposition of graphitic carbon nitride (g-C3N4) films on biomass substrate: optoelectronic performance evaluation and life cycle assessment, Advanced Composites and Hybrid Materials 5(2) (2022) 813-822.
[61] M. Lian, Y. Huang, Y. Liu, D. Jiang, Z. Wu, B. Li, Q. Xu, V. Murugadoss, Q. Jiang, M. Huang, Z. Guo, An overview of regenerable wood-based composites: preparation and applications for flame retardancy, enhanced mechanical properties, biomimicry, and transparency energy saving, Advanced Composites and Hybrid Materials 5(3) (2022) 1612-1657.
[62] A.I. Sema, J. Khatri, B.B. Dhar, G. Kulsi, J. Bhattacharyya, On the Utility of Teakwood Biochar for Iron Contaminants Removal from Water, ES Materials & Manufacturing in press (2023) http://dx.doi.org/10.30919/esmm5f871.
[63] Z. Sun, Y. Zhang, S. Guo, J. Shi, C. Shi, K. Qu, H. Qi, Z. Huang, V. Murugadoss, M. Huang, Z. Guo, Confining FeNi nanoparticles in biomass-derived carbon for effectively photo-Fenton catalytic reaction for polluted water treatment, Advanced Composites and Hybrid Materials 5(2) (2022) 1566-1581.
[64] Z. Wang, K. Yin, Y. Zhang, K. Sun, L. Xie, M. Cong, S. Cao, Y. Lei, X. Li, R. Fan, Two-dimensional Ti3C2Tx/carbonized wood metacomposites with weakly negative permittivity, Advanced Composites and Hybrid Materials 5(3) (2022) 2369-2377.
[65] A. Vijeata, G.R. Chaudhary, A. Umar, S. Chaudhary, Distinctive Solvatochromic Response of Fluorescent Carbon Dots Derived from Different Components of Aegle Marmelos Plant, Engineered Science 15 (2021) 197-209.
[66] H. Zhang, J. Yu, J. Wang, Non-Thermal Oxygen-Helium Plasma Modification and Regeneration of Sawdust Biochar to Promote Aniline Removal, ES Energy & Environment 15 (2022) 15-27.
[67] F. Kang, X. Jiang, Y. Wang, J. Ren, B.B. Xu, G. Gao, Z. Huang, Z. Guo, Electron-rich biochar enhanced Z-scheme heterojunctioned bismuth tungstate/bismuth oxyiodide removing tetracycline, Inorganic Chemistry Frontiers 10 (2023) 6045-6057.
[68] C. Xiong, Q. Xiong, M. Zhao, B. Wang, L. Dai, Y. Ni, Recent advances in non-biomass and

biomass-based electromagnetic shielding materials, Advanced Composites and Hybrid Materials 6(6) (2023) 205.
[69] K. Zhou, Y. Sheng, W. Guo, L. Wu, H. Wu, X. Hu, Y. Xu, Y. Li, M. Ge, Y. Du, X. Lu, J. Qu, Biomass porous carbon/polyethylene glycol shape-stable phase change composites for multi-source driven thermal energy conversion and storage, Advanced Composites and Hybrid Materials 6(1) (2023) 34.
[70] W. Li, H. Qi, F. Guo, Y. Du, N. Song, Y. Liu, Y. Chen, Co nanoparticles supported on cotton-based carbon fibers: A novel broadband microwave absorbent, Journal of Alloys and Compounds 772 (2019) 760-769.
[71] H.-B. Zhao, J.-B. Cheng, Y.-Z. Wang, Biomass-derived Co@crystalline carbon@carbon aerogel composite with enhanced thermal stability and strong microwave absorption performance, Journal of Alloys and Compounds 736 (2018) 71-79.
[72] T. Gao, Y. Ma, L. Ji, Y. Zheng, S. Yan, Y. Li, X. Zhang, Nickel-coated wood-derived porous carbon (Ni/WPC) for efficient electromagnetic interference shielding, Advanced Composites and Hybrid Materials 5(3) (2022) 2328-2338.
[73] C. Liu, Y. Tong, C. Liu, J. Liu, H. Sun, Q. Hu, S. Wu, Y. Zhao, J. Li, X. Guo, Y. Feng, Novel and efficient electromagnetic wave absorption of SiBCN(Fe) nanofibers, Colloids and Surfaces A: Physicochemical and Engineering Aspects 679 (2023) 132605.
[74] S. Gao, Q. An, Z. Xiao, S. Zhai, Z. Shi, Significant promotion of porous architecture and magnetic Fe3O4 NPs inside honeycomb-like carbonaceous composites for enhanced microwave absorption, RSC Advances 8(34) (2018) 19011-19023.
[75] Q. Yang, Y. Shi, Y. Fang, Y. Dong, Q. Ni, Y. Zhu, Y. Fu, Construction of polyaniline aligned on magnetic functionalized biomass carbon giving excellent microwave absorption properties, Composites Science and Technology 174 (2019) 176-183.
[76] R. Liu, H. Zhu, Z. Zhu, Construction of the sandwich magnetic FeNi@C@Fe3O4 powders with the characteristics of lower density and broadband absorption, Colloids and Surfaces A: Physicochemical and Engineering Aspects 652 (2022) 129778.
[77] Y. Huang, G. Liu, D. Liu, M. Hao, P. Xie, Z. Shi, G. Lin, Excellent Microwave Absorption Performance in Porous Co/C Nanocomposites by Biomass Conversion, ES Food & Agroforestry 12 (2023) 888.
[78] H. Liang, H. Xing, M. Qin, H. Wu, Bamboo-like short carbon fibers@Fe3O4@phenolic resin and honeycomb-like short carbon fibers@Fe3O4@FeO composites as high-performance electromagnetic wave absorbing materials, Composites Part A: Applied Science and Manufacturing 135 (2020) 105959.
[79] G. Zucchelli, R.C. Jennings, F.M. Garlaschi, Independent fluorescence emission of the chlorophyll spectral forms in higher plant Photosystem II, Biochimica et Biophysica Acta (BBA) - Bioenergetics 1099(2) (1992) 163-169.
[80] Y. Liu, Z. Chen, W. Xie, S. Song, Y. Zhang, L. Dong, In-Situ Growth and Graphitization Synthesis of Porous Fe3O4/Carbon Fiber Composites Derived from Biomass as Lightweight Microwave Absorber, ACS Sustainable Chemistry & Engineering 7(5) (2019) 5318-5328.
[81] W. Gu, J. Sheng, Q. Huang, G. Wang, J. Chen, G. Ji, Environmentally Friendly and

Multifunctional Shaddock Peel-Based Carbon Aerogel for Thermal-Insulation and Microwave Absorption, Nano-Micro Letters 13(1) (2021) 102.
[82] R. Shu, W. Li, Y. Wu, J. Zhang, G. Zhang, M. Zheng, Fabrication of nitrogen-doped cobalt oxide/cobalt/carbon nanocomposites derived from heterobimetallic zeolitic imidazolate frameworks with superior microwave absorption properties, Composites Part B: Engineering 178 (2019) 107518.
[83] G. Wu, Y. Cheng, Y. Ren, Y. Wang, Z. Wang, H. Wu, Synthesis and characterization of γ-Fe2O3@C nanorod-carbon sphere composite and its application as microwave absorbing material, Journal of Alloys and Compounds 652 (2015) 346-350.
[84] H. Lv, X. Liang, Y. Cheng, H. Zhang, D. Tang, B. Zhang, G. Ji, Y. Du, Coin-like α-Fe2O3@CoFe2O4 Core–Shell Composites with Excellent Electromagnetic Absorption Performance, ACS Applied Materials & Interfaces 7(8) (2015) 4744-4750.
[85] T. Hou, B. Wang, M. Ma, A. Feng, Z. Huang, Y. Zhang, Z. Jia, G. Tan, H. Cao, G. Wu, Preparation of two-dimensional titanium carbide (Ti3C2Tx) and NiCo2O4 composites to achieve excellent microwave absorption properties, Composites Part B: Engineering 180 (2020) 107577.
[86] X. Yu, Y. Zhang, L. Wang, L. Xing, W. You, J. Liu, G. Chen, G. Ding, J. Ding, X. Liu, M. Wang, R. Che, Improved microwave absorption performance of a multi-dimensional Fe2O3/CNTCM@CN assembly achieved by enhanced dielectric relaxation, Journal of Materials Chemistry C 8(17) (2020) 5715-5726.
[87] Y. Qiu, Y. Lin, H. Yang, L. Wang, M. Wang, B. Wen, Hollow Ni/C microspheres derived from Ni-metal organic framework for electromagnetic wave absorption, Chemical Engineering Journal 383 (2020) 123207.
[88] X. Zhang, Y. Dong, F. Pan, Z. Xiang, X. Zhu, W. Lu, Electrostatic self-assembly construction of 2D MoS2 wrapped hollow Fe3O4 nanoflowers@1D carbon tube hybrids for self-cleaning high-performance microwave absorbers, Carbon 177 (2021) 332-343.
[89] T. Liu, X. Xie, Y. Pang, S. Kobayashi, Co/C nanoparticles with low graphitization degree: a high performance microwave-absorbing material, Journal of Materials Chemistry C 4(8) (2016) 1727-1735.
[90] J. Luo, K. Zhang, M. Cheng, M. Gu, X. Sun, MoS2 spheres decorated on hollow porous ZnO microspheres with strong wideband microwave absorption, Chemical Engineering Journal 380 (2020) 122625.
[91] H. Zhao, X. Xu, Y. Wang, D. Fan, D. Liu, K. Lin, P. Xu, X. Han, Y. Du, Heterogeneous Interface Induced the Formation of Hierarchically Hollow Carbon Microcubes against Electromagnetic Pollution, Small 16(43) (2020) 2003407.
[92] B. Wang, H. Liao, X. Xie, Q. Wu, T. Liu, Bead-like cobalt nanoparticles coated with dielectric SiO2 and carbon shells for high-performance microwave absorber, Journal of Colloid and Interface Science 578 (2020) 346-357.
[93] L. Lei, Z. Yao, J. Zhou, W. Zheng, B. Wei, J. Zu, K. Yan, Hydrangea-like Ni/NiO/C composites derived from metal-organic frameworks with superior microwave absorption, Carbon 173 (2021) 69-79.
[94] H. Guan, H. Wang, Y. Zhang, C. Dong, G. Chen, Y. Wang, J. Xie, Microwave absorption

performance of Ni(OH)2 decorating biomass carbon composites from Jackfruit peel, Applied Surface Science 447 (2018) 261-268.
[95] X. Zhao, J. Yan, Y. Huang, X. Liu, L. Ding, M. Zong, P. Liu, T. Li, Magnetic porous CoNi@C derived from bamboo fiber combined with metal-organic-framework for enhanced electromagnetic wave absorption, Journal of Colloid and Interface Science 595 (2021) 78-87.
[96] X. Wang, F. Pan, Z. Xiang, Q. Zeng, K. Pei, R. Che, W. Lu, Magnetic vortex core-shell Fe3O4@C nanorings with enhanced microwave absorption performance, Carbon 157 (2020) 130-139.
[97] X. Zeng, X. Cheng, R. Yu, G.D. Stucky, Electromagnetic microwave absorption theory and recent achievements in microwave absorbers, Carbon 168 (2020) 606-623.
[98] J.A. Marins, B.G. Soares, H.S. Barud, S.J.L. Ribeiro, Flexible magnetic membranes based on bacterial cellulose and its evaluation as electromagnetic interference shielding material, Materials Science and Engineering: C 33(7) (2013) 3994-4001.

Declaration of interests

The authors declare that they have no known competing financial interests or personal relationships that could have appeared to influence the work reported in this paper.

Research Highlights

- A Fe_3O_4 and spinach stems-derived carbon composite was prepared.
- The composites show excellent wave absorption properties
- The minimal RL value of -48.81dB and bandwidth of 4.77GHz were observed.

Graphical Abstract